INSTITUTE OF PHYSICS PUBLISHING SEMICONDUCTOR SCIENCE AND TECHNOLOGY
Semicond. Sci. Technol. **20** (2005) 1149–1152 doi:10.1088/0268-1242/20/11/009

980-nm DBR lasers using higher order gratings defined by i-line lithography

J Fricke, H Wenzel, M Matalla, A Klehr and G Erbert

Ferdinand-Braun-Institut für Höchstfrequenztechnik, Gustav-Kirchhoff-Straße 4, 12489 Berlin, Germany

E-mail: fricke@fbh-berlin.de

Received 30 May 2005, in final form 20 September 2005
Published 18 October 2005
Online at stacks.iop.org/SST/20/1149

Abstract
We report on the simultaneous definition and fabrication of Bragg gratings and ridge waveguides using wafer stepper lithography and reactive ion etching, respectively. Single-longitudinal mode emission from two-section ridge-waveguide distributed feedback lasers with sixth and seventh order gratings will be reported. This technology enables a cheap fabrication of wavelength-stabilized lasers and a simple variation of the parameters of the gratings on the wafer using optical lithography.

(Some figures in this article are in colour only in the electronic version)

1. Introduction

Wavelength-stabilized semiconductor lasers find widespread application in optical communication, spectroscopy, nonlinear frequency conversion and the excitation of electronic transitions in atoms. Wavelength stabilization realized by means of gratings in external cavity configurations is expensive and sensitive to acoustic, thermal and vibrational perturbations. These difficulties are avoided if the Bragg grating is integrated in the semiconductor chip, which results in distributed Bragg reflector (DBR) or distributed feedback (DFB) lasers. However, their fabrication involves complicated multiple growth and processing steps, which lengthen cycle times and drive down yields leading to higher costs.

Having this in mind, single-growth DFB and DBR lasers are advantageous compared to multiple-growth devices. However, the laterally coupled [1] or deeply etched gratings [2] used in single-growth devices are mostly based on electron-beam [3] or focused-ion-beam lithography [4], which are slow and expensive technologies. In [5] a surface grating was fabricated using holographic lithography which is more cost effective. However, an additional grating recess etch step had to be performed.

Hence, the problem of multiple processing steps has not so far been solved. The reason is that typical gratings exploit the first to third Bragg orders, leading to grating periods between 100 and 500 nm for the lasing wavelengths between 800 and 1000 nm which we are interested in. The fabrication of these small structures can hardly be combined with standard semiconductor processing methods.

In this paper, we use sixth and seventh order surface gratings etched down to the p-waveguide layer having appropriate duty cycles around 0.9. In this way we obtain sufficiently large reflection coefficients for the DBRs. The large periods of around 1 μm enable a common fabrication of Bragg gratings and ridge-waveguides for lateral optical confinement in a single lithography step as well as a single etching step.

This paper is organized as follows. The results of a computation of the reflectivity of deeply etched higher order Bragg gratings are given in section 2. The fabrication details and experimental results of devices having different lengths of the DBR section are presented in sections 3 and 4, respectively. The paper is concluded in section 5.

2. Theoretical considerations

In order to determine the optimum geometrical and technological parameters, we computed reflectivity spectra of deeply etched DBRs in dependence of length L_{DBR} of the DBR, Bragg order, duty cycle and residual layer thickness, assuming a rectangular shape of the Bragg gratings. The duty cycle is the ratio between the length of the unetched region and the Bragg period. In the computations, the Bragg period is kept constant for the given Bragg order. The gratings are assumed to be infinitely extended into the lateral direction. Thus, the DBRs can be modelled as a stack of slab waveguides.

The calculations were carried out with the simulation tool CAMFR [6]. In CAMFR, the field in each slab is expanded

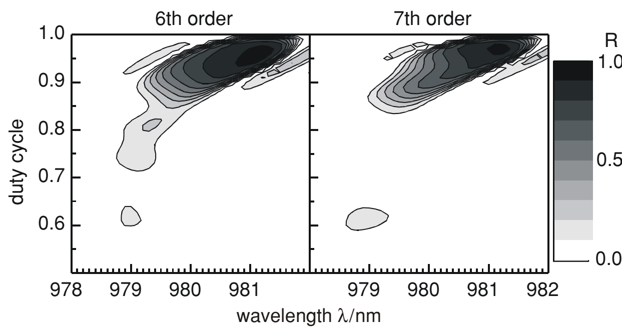

Figure 1. A grey-scale contour plot of the reflectivity of 200 μm long sixth (left) and seventh (right) order gratings versus duty cycle and wavelength, computed with the CAMFR simulation tool.

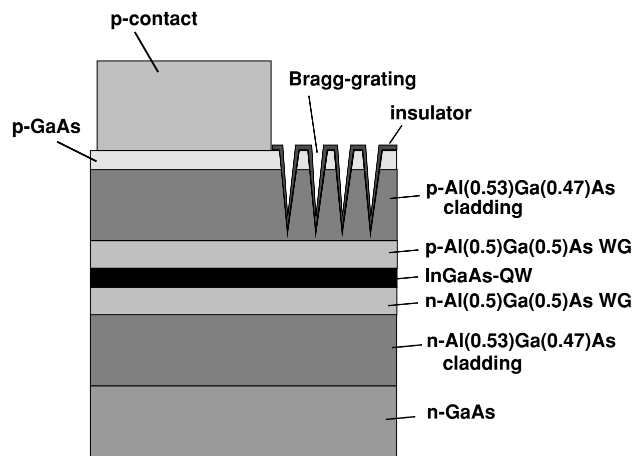

Figure 2. A schematic picture of the epitaxial layer sequence and the Bragg gratings of the DBR lasers.

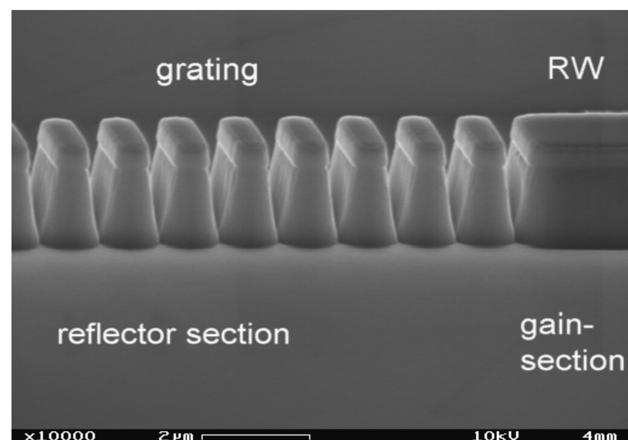

Figure 3. Scanning electron microscope picture of the dry-etched RW with and without Bragg gratings, covered by a 100 nm isolation layer.

onto the eigenmodes in that slab. In order to get a discrete set of the radiation modes, the slabs are bounded by electric walls. Parasitic reflections eliminated by perfectly matched layers (PMLs) are placed at the walls. A total number of 100 eigenmodes were used in the simulation. At the interfaces between the slabs, the transition conditions for the electric and magnetic field components give rise to reflection and transmission matrices. The propagation of the fields from one interface to the other interface is given by diagonal propagation matrices. As described in [6], the reflection and transmission matrices of the entire finite periodic gratings are recursively obtained by the so-called S-matrix algorithm. The accurateness of the simulation tool was demonstrated in [7].

The slab waveguides underlying the computations are based on an epitaxial layer structure, which has already been used for high-power Fabry–Perot ridge-waveguide (RW) lasers [8]. It consists of an active InGaAs single quantum well (QW) embedded in a 250-nm thick $Al_{0.50}Ga_{0.50}As$ waveguide and $Al_{0.53}Ga_{0.47}As$ cladding layers. In the etched regions, the removed $Al_{0.53}Ga_{0.47}As$ was substituted by SiN.

Greyscale contour plots of the computed reflectivity spectra of the fundamental mode versus duty cycle are shown in figure 1 for a 200 μm long DBR with sixth and seventh order gratings. The residual layer thickness above the active layer is 300 nm. As can be seen from the figure, a reflection coefficient greater than 50% can be achieved with duty cycles greater than 0.9 for both Bragg orders. The maximum reflectivity reaches 92% independent of the Bragg order. For duty cycles smaller than 0.8, the reflectivity vanishes almost completely. This behaviour is due to the fact that only in the case of duty cycles approaching 1, where most of the stack consists of the unetched waveguide, the fundamental mode spreads deep into the AlGaAs and SiN cladding layers and is strongly affected by the difference in the corresponding refractive indices.

3. Fabrication

The DBR RW lasers are based on the epitaxial layer structure described in section 2. It is grown in a single step by metal-organic chemical vapour epitaxy (MOVPE). The active layer was not removed in the passive sections.

The processing of the lasers started with the deposition of a 600-nm thick photoresist layer and subsequent exposure by an i-line wafer stepper to define both the RW and the Bragg grating structures at the same time. Aiming for an emission wavelength of 980 nm, periods of 914.5 and 1067 nm were chosen for the sixth and seventh order Bragg gratings, respectively. These periods are large enough to use an i-line wafer stepper providing there is a resolution limit of 400 nm. Hence, they can be very precisely adjusted over the whole wafer. The width of the RW was chosen to be 2 μm. After developing the photoresist, the grating and RW structures were simultaneously transferred into the epitaxial layer structure with a reactive ion etching (RIE) process using a BCl_3/Ar plasma. The etch depth of about 2 μm ensured that, above the active layer, only a 250-nm thick p-waveguide layer remained in the grooves after etching. A schematic picture showing the epitaxial layer sequence and the placement of the Bragg gratings is given in figure 2. In order to achieve the desired duty cycle of around 0.9, the etching parameters were chosen in such a way that V-shaped grooves were obtained (compare the SEM picture of parts of the reflector section and ridge waveguide in figure 3).

The Bragg gratings were realized in parts of the RW only. The results are DBR lasers with two sections, namely, a gain section without Bragg gratings and a reflector section with a

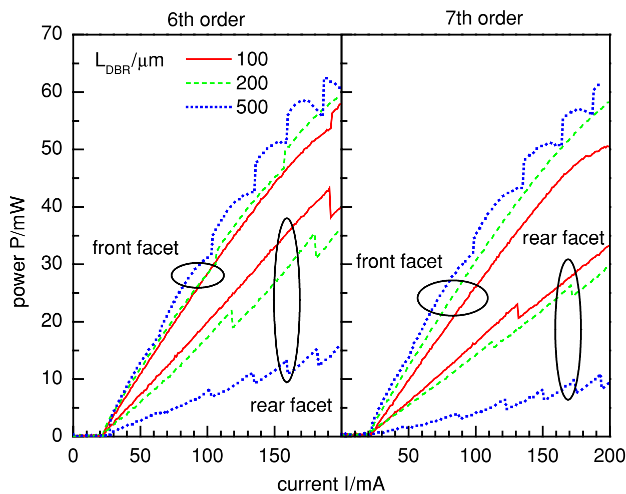

Figure 4. Light–current characteristics of 1.5 mm long uncoated DBR lasers having sixth (left) and seventh (right) order gratings. The parameter is the length of the DBR section in μm. The output powers emitted from gain (front facet) and reflector sections (rear) are given.

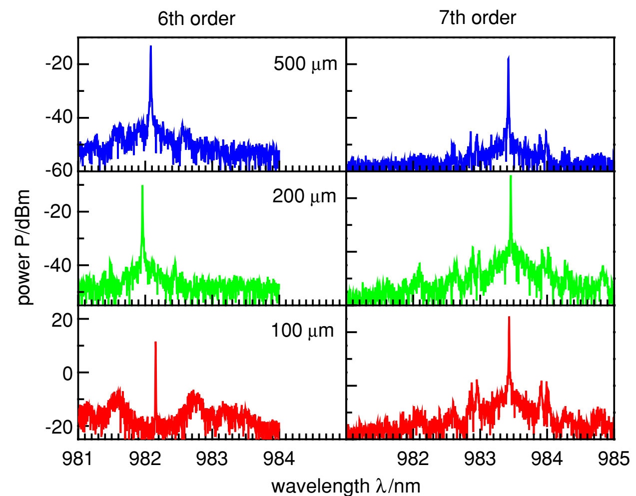

Figure 5. Optical spectra of the DBR lasers of figure 2 having sixth (left) and seventh (right) order gratings for different lengths of the DBR section, measured at a current of 200 mA.

Bragg grating. The length L_{DBR} of the reflector section was varied between 100 and 500 μm. The total cavity length was kept constant at $L = 1500$ μm. It should be noted that laterally there are no gratings, as can be seen from figure 3 which shows parts of the RW with and without Bragg gratings. The different layers visible in figure 3 are the contact and cladding layers, covered by an insulator (SiN).

After removing the photoresist, an isolation layer was deposited and opened at the top of the RW, followed by the deposition of the p-electrode and electroplating of gold in the gain section. Finally, the wafer was thinned and the n-electrode was deposited on the back side of the wafer. The lasers of a bar were not separated in the present study, and for the measurements, the bars were attached to copper heat sinks.

4. Results

The measurements of the total optical power and the optical spectra were carried out in continuous wave (CW) operation at room temperature using a calibrated integrating sphere. Only the gain sections were contacted and biased; the reflector sections acted purely passively. The light–current (L–I) characteristics of uncoated 1.5 mm long DBR lasers with sixth and seventh order gratings and three different lengths (L_{DBR}) of DBR section are shown in figure 4. The upper and lower three curves depict the power (P) emitted from the gain (front facet) and reflector sections (rear facet), respectively.

Comparing the left and right parts of figure 4, it can be concluded that the L–I characteristics do not depend on the Bragg orders investigated. The threshold currents of about 20 mA and the output powers at 200 mA are nearly the same for both types of DBR lasers. Moreover, the distribution of the output power between the front and rear facets and its dependence on the L_{DBR} is very similar, too. The slope efficiency (S) of the devices with 200 μm long reflector sections is about 0.38 WA^{-1} up to $P = 40$ mW.

The kinks in the L–I characteristics are typical for DBR lasers. They are caused by a thermal detuning of the gain and reflector sections and are connected with a mode hop. It is interesting to note that at the front facet a mode hop results in an increase of the power. However, at the rear facet the power decreases. The reason is that with increasing current through the gain section the lasing mode is shifted away from the spectral maximum of the reflectivity of the DBR. Hence, the slope efficiency at the front (rear) facet decreases (increases) until the mismatch between the wavelengths of the lasing mode and the reflection peak is too large. Thus, the mode hop is also correlated with a change in the longitudinal power profile of the lasing mode. The number of mode hops decreases with a reduction of the L_{DBR} caused by a widening and decrease of the reflectivity.

The optical spectra of the DBR lasers in figure 5 were measured at a current of 200 mA. They reveal single-longitudinal mode emission for both Bragg orders and all three lengths of the reflector section, despite the fact that the devices are as cleaved. The side-mode suppression ratio (SMSR) exceeds 30 dB, limited by the dynamic range of the optical spectrum analyser (Advantest Q8347) used. Note that there is a difference in the lasing wavelengths between the devices with sixth and seventh order gratings of more than 1 nm, although both Bragg gratings were fabricated in the nominally same manner. This can be explained with the help of the contour plot in figure 1, where a shift in the wavelength of the maximum reflectivity versus duty cycle can be observed due to the variation of the average effective index determining the Bragg wavelength. Please note the V-shape of the grooves, which makes it difficult to assign a duty cycle.

From figure 5 it can be seen that there are small differences in the lasing wavelength and also between the devices of the same grating order, but with different lengths of the reflector section. This can be attributed to the fact that up to a current of 200 mA the devices passed a different number of mode hops. Furthermore, due to the correspondingly different lengths of the gain section, the thermal behaviour of the devices differs,

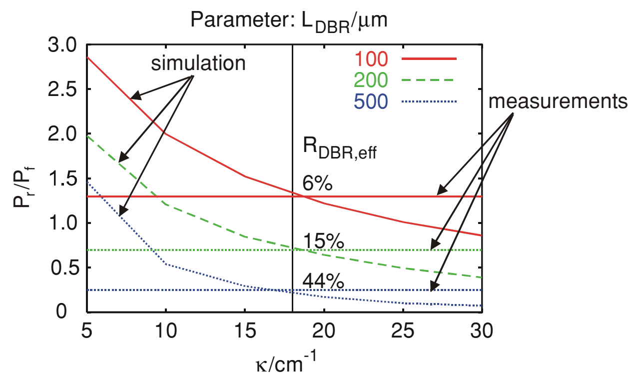

Figure 6. The ratio between the power emitted at the rear facet and the power emitted at the front facet of 1.5 mm long DBR lasers low and anti-reflection coated (reflectivities $R_f = 10\%$, $R_r = 0\%$). Horizontal lines: measured values. Curves: calculated values versus coupling coefficient. The parameter is the length of the DBR section.

which also influences the lasing wavelength. The detuning between the Bragg wavelength and the gain peak wavelength, $\Delta\lambda = \Delta\lambda_{Bragg} - \Delta\lambda_{gain}$, varied between −4 and +9 nm on different wafers. Both the *L–I* characteristics as well as the optical spectra of devices fabricated from these wafers showed operation in a mode determined by the Bragg gratings.

In order to estimate the achieved reflectivity of the Bragg gratings, the facet of the reflector section (rear facet) of 1.5 mm long DBR lasers was anti-reflection coated. The reflectivity of the facet of the gain section (front facet) was chosen to be 10%. The output powers P_f and P_r at the facets were measured for the different lengths L_{DBR} and the ratio P_r/P_f was plotted at horizontal lines in figure 6. The power-current characteristics of the laser were additionally simulated according to the scheme described in [9]. Thereby, the coupling coefficient κ of the grating was varied and the ratio P_r/P_f was again plotted in figure 6. As can be seen, the experimental horizontal lines and the theoretical curves cross at a coupling coefficient of about 18 cm^{-1} for all lengths of the reflector section. The corresponding effective reflection coefficients of the DBRs are 6%, 15% and 44% for L_{DBR} equal to 100, 200 and 500 μm, respectively. These values are smaller than what can be theoretically achieved according to figure 1, which could be due to the V-shape of the grooves which makes it difficult to assign a duty cycle. Furthermore, due to the RW the mode is also confined laterally, which leads to the reduction of the reflectivity of a DBR [10] and which was not accounted for in the simulations performed with CAMFR.

5. Conclusions

For the first time, the successful fabrication of single-growth DBR RW lasers utilizing sixth and seventh order Bragg gratings etched down to the p-waveguide was demonstrated. These higher order Bragg gratings, defined together with the RW by projection lithography using a wafer stepper, yield sufficient reflectivity for longitudinal single-mode operation of uncoated lasers with a SMSR greater than 30 dB. The investigated uncoated devices exhibit a *L–I* characteristic typical for DBR lasers with an output power of 60 mW at a current of 200 mA. The technology allows highly flexible, low-cost manufacturing of wavelength-stabilized lasers.

Theoretical investigations using a bi-directional mode-expansion tool indicate the necessity for careful adjustment of the duty cycle in the range 0.9 to 0.95 for higher order Bragg gratings in order to obtain a sufficiently large reflectivity. However, this adjustment can be partially avoided by the V-shaped grooves realized in the fabrication process which can be assigned a continuously varying duty cycle.

Acknowledgments

The authors thank H Götzelt for wafer processing, J Hopp for performing the measurements and P Bienstman (Ghent University) for providing the CAMFR tool. This work was supported by Zukunftsfonds Berlin.

References

[1] Martin R D, Fourouhar S, Keo S, Lang R J, Hunsperger R G, Tiberio R C and Chapman P F 1995 *IEEE Photon. Technol. Lett.* **7** 244
[2] Wiedemann J, Ebihara K, Kim H C, Chen B, Ohta B, Matsui K, Tamura S, Shim J L and Arai S 2001 *Electron. Lett.* **37** 831
[3] Roh S D, Hughes J S, Lammert R M, Osowski M L, Beernink K J, Papaen G C and Coleman J J 1997 *IEEE Photon. Technol. Lett.* **9** 285
[4] Rennon S, Bach L, Reithmaier J P and Forchel A 2001 *IEEE J. Select. Top. Quantum Electron.* **7** 306
[5] Hofstetter D, Zappe H P, Epler J E and Söchtig J 1994 *Electron. Lett.* **30** 1858
[6] Bienstman P and Baets R 2001 *Opt. Quantum Electron.* **33** 327
[7] Čtyroký J *et al* 2002 *Opt. Quantum Electron.* **34** 455
[8] Beister G, Bugge F, Erbert G, Maege J, Ressel P, Sebastian J, Thies A and Wenzel H 1998 *Electron. Lett.* **34** 778
[9] Wünsche H J, Bandelow U and Wenzel H 1993 *IEEE J. Quantum Electron.* **29** 1751
[10] Kasunic K J 2000 *J. Lightwave Technol.* **18** 425